

## Article

# Influence of Technological Factors on the Formation and Transformation of Iron-Containing Phases in the Process of Ferritization of Exhausted Etching Solutions

Dmitry Samchenko <sup>1</sup>, Gennadii Kochetov <sup>1</sup>, Yuliia Trach <sup>2,3,\*</sup> , Denys Chernyshev <sup>1</sup>  and Andriy Kravchuk <sup>1</sup>

<sup>1</sup> Faculty of Engineering Systems and Ecology, Kyiv National University of Construction and Architecture, 03680 Kyiv, Ukraine; sama30071988@gmail.com (D.S.); gkochetov@gmail.com (G.K.); kravchuk.am@knuba.edu.ua (A.K.)

<sup>2</sup> Institute of Agroecology and Land Management, National University of Water and Environmental Engineering, 33028 Rivne, Ukraine

<sup>3</sup> Faculty of Civil and Environmental Engineering, Institute of Civil Engineering, Warsaw University of Life Sciences, 02-787 Warsaw, Poland

\* Correspondence: y.p.trach@nuwm.edu.ua

**Abstract:** Every year, metallurgical enterprises generate a massive amount of toxic exhausted high-concentration etching solutions. Application of the ferritization process to recycle exhausted etching solutions can help to prevent environmental pollution. It enables a cost-efficient use of water at an industrial plant and allows the plant to obtain products from toxic industrial waste and utilize it. The aim of the study was to analyze the qualitative and quantitative composition of the formed sediment and its grain size composition. Variable study parameters were the initial pH values of the solutions, the initial concentrations of total iron, and the duration of the aeration process of the reaction mixture. Thermal activation and alternating magnetic fields were used to activate the ferritization. The XRD showed that the formed sediments contained phases of  $\gamma$ -FeOOH,  $\delta$ -FeOOH,  $\text{Fe}_3\text{O}_4$ , and  $\gamma$ - $\text{Fe}_2\text{O}_3$ . Granulometry analysis showed that these sediments were highly dispersed and heterogeneous. Chemically stable phases of magnetite were obtained in the composition of sediments, with an initial concentration of iron in the reaction mixture of  $16.6 \text{ g/dm}^3$ , a pH of 11.5, and a process duration of 15 min. The study results demonstrated the feasibility of further study and possible use of such sediments with a high magnetite content for the production of materials with ferromagnetic and sorption properties.

**Keywords:** ferritization; etching solutions; magnetite; total iron; phase transitions



**Citation:** Samchenko, D.; Kochetov, G.; Trach, Y.; Chernyshev, D.; Kravchuk, A. Influence of Technological Factors on the Formation and Transformation of Iron-Containing Phases in the Process of Ferritization of Exhausted Etching Solutions. *Water* **2024**, *16*, 1085. <https://doi.org/10.3390/w16081085>

Academic Editor: Yujue Wang

Received: 12 January 2024

Revised: 22 February 2024

Accepted: 4 April 2024

Published: 10 April 2024



**Copyright:** © 2024 by the authors. Licensee MDPI, Basel, Switzerland. This article is an open access article distributed under the terms and conditions of the Creative Commons Attribution (CC BY) license (<https://creativecommons.org/licenses/by/4.0/>).

## 1. Introduction

Every year, hundreds of millions of tons of toxic exhausted highly concentrated etching solutions are formed at enterprises in the metallurgical, chemical, machine-building, and other industries of Eastern Europe and Asia [1,2]. Steel mills in the European Union (EU) generate 300,000 cubic meters of exhausted etching solutions (EES) annually, with 150,000 tons being stored. The etching process is crucial for achieving a high-quality steel surface for subsequent processing [3]. To remove the scale, which contains oxides, acids are used. Etching solutions are deemed exhausted when the acid concentration drops by 75–85%, resulting in a metal content increase of up to  $150\text{--}250 \text{ g/dm}^3$  [4]. Due to decreasing etching efficiency with rising dissolved metal content in the bath, exhausted bath solutions must be discarded.

Additionally, the steel etching process contributes to the formation of highly polluted wastewater (up to  $204 \text{ g/dm}^3$  of Fe(III) and up to  $110 \text{ g/dm}^3$  of Zn(II)) [5]. Zinc leaching and the resulting residues with high iron contamination pose another challenge. This leads to substantial metal losses and secondary environmental contamination. The recovery of

zinc, iron, and mineral acids is a major environmental concern due to the acidic nature of the waste [6].

These solutions are formed during the processing of steel products, usually with a solution of sulfuric acid in order to remove the scale and rust from their surface. Exhausted sulfuric acid-based etching solution, depending on the composition and condition of the processing of steel parts, contains up to 300 g/dm<sup>3</sup> of iron sulfate FeSO<sub>4</sub> [7,8]. Given this, special attention is paid to the development and introduction of technologies for the neutralization and integrated processing of liquid iron-containing wastes from metallurgical, chemical, and other industries. Such measures will allow us to address two problems in parallel: environmentally sound waste disposal and the generation of raw materials for the production of useful products.

The current state of recycling and disposal is subject to processing small amounts of exhausted solutions after the etching of steel surfaces, resulting in the accumulation of these wastes. On many industrial sites, these highly concentrated solutions are not always treated to the required level for reuse. As a result, thousands of tons of toxic iron-containing compounds enter water bodies with insufficiently treated wastewater. Iron ions have high migratory mobility, the ability to accumulate in living organisms, and can cause various physiological disorders.

An analysis of research work on the processing of such acidic iron-containing wastewater indicates the relevance and feasibility of research efforts in this direction [9]. Methods of obtaining chemically stable and low-toxic substances such as magnetite Fe<sub>3</sub>O<sub>4</sub> and maghemite  $\gamma$ -Fe<sub>2</sub>O<sub>3</sub> from such wastes are of particular interest since they have the highest magnetic susceptibility among iron oxides. These compounds have the structure of an inverted spinel, but maghemite is distinguished by the presence of free vacancies distributed in the cationic sublattice. Magnetite Fe<sub>3</sub>O<sub>4</sub> and maghemite  $\gamma$ -Fe<sub>2</sub>O<sub>3</sub> have a wide range of applications, including the manufacture of magnetic carriers, sensors, auxiliary colloidal substances for drugs, catalysts, and construction materials [10,11].

Another promising direction for utilization of these iron-containing, magnetic materials is associated with their use as sorbents for the removal of metals and organic substances from wastewater flows. Iron-rich natural materials such as volcanic tuff, some kaolins, zeolites, and others that contain hematite (Fe<sub>2</sub>O<sub>3</sub>) have shown a higher adsorption capacity for heavy metals compared to those materials that do not contain them or contain them in very low concentrations. So, for example, the sorption capacity of Mn<sup>2+</sup> by iron-containing tuff is more than 8.5 mg/g, and by basalt, it is 4.3 mg/g [12,13]. In addition, in the research study that compared the Ni<sup>2+</sup> sorption capacity of different kaolins, it was found that with hematite content in kaolin over 3.5%, the sorption capacity was approximately 2.5 times higher [14].

Numerous dispersed nanoparticles possess exceptional adsorption properties and offer several advantages over traditional adsorbents. However, some concerns arise regarding their potential toxicity due to their inherent structure, size, and other chemical and physical characteristics, even at low concentrations [15]. Consequently, the development of effective procedures and technical solutions for the separation of these nanomaterials from water becomes imperative. In addressing this challenge, it is the utilization of magnetite nanoparticles or their modified forms that stands out as the most practical solution. Magnetite nanoparticles exhibit superparamagnetic behavior, meaning they are readily attracted to an applied magnetic field but retain no residual magnetism once the field is removed [16]. Moreover, the ability to recover and reuse magnetite adsorbents after desorption of adsorbed dye molecules enables their repeated application in successive adsorption cycles. These attributes render magnetite nanoparticles attractive candidates for facile, efficient, economical, and large-scale removal of dye molecules from aqueous samples [17].

Analyzing the research results on the adsorption of various (cationic and anionic) pollutants by various iron-containing adsorbents with or without magnetic properties, we can identify their particular advantage [18–20]. It mainly consists of the fact that such

materials are able to purify water in a wide range of pH values. This is due to the relatively high value of  $pH_{pzc}$  (more than 8.2) [14,21].

Currently, there are various methods for obtaining highly dispersed iron-containing powders and composites based on them [22]. Most of the methods are based on solid-phase interaction of oxides, hydroxides, or salts of heavy metals, which requires expensive precursors and significant energy costs. In particular, the process of forming magnetite and maghemite is carried out at temperatures above 400 °C and takes 4–5 h [23]. Samples of iron-containing powder obtained by this method had a dispersed structure [24]. However, it should be noted that the production of such materials by the method of high-temperature decomposition of iron-containing compounds, using organic solvents and surfactants to stabilize and prevent the agglomeration of highly dispersed particles of iron oxides, is quite effective, but resource-intensive and does not provide the ability to control their size and shape.

The hydrophase ferritization method is an economical and easy-to-operate method for processing liquid iron-containing waste to produce magnetic materials [25,26]. The essence of this method is the partial oxidation of  $Fe^{2+}$  ions to  $Fe^{3+}$  by aeration with atmospheric oxygen and their subsequent precipitation in an alkaline medium. The ferritization process promotes the rapid formation of dispersed substances with magnetic properties. The disadvantages of traditional ferritization are its temperature requirements—temperatures above 75 °C. In research paper [27], it was shown that an alternative to thermal ferritization is the activation of the reaction mixture with alternating magnetic fields (AMF) at ambient temperatures. Using this activation method, in research paper [28], iron-containing ferromagnetic compounds of various phase compositions were obtained from liquid industrial waste, the structure of which contains nickel, zinc, and copper ions.

The course of the ferritization process is influenced by a number of technological factors that determine the type of primary embryonic iron-containing structures, their formation, and further development with the formation of stable compounds with different particle sizes and shapes. Among these factors are the initial concentration of iron ions [29], the pH value [30], the temperature [31,32], the process duration [33], and the oxidizer (air oxygen) consumption [34]. In addition, the above factors can affect the formation of a certain modification of iron hydroxides and oxyhydroxides and their subsequent transformation into other more stable oxide compounds in an alkaline medium [35].

There are situations where only dispersed materials with ferromagnetic properties can be used for water treatment, and such sorbents need to be additionally provided. Known methods of their synthesis are the dry process, wet chemical process, and microbial process [18,36]. Properties and shapes of the dispersed sediments formed depend on the conditions provided during the reaction, such as the type of salts used, the ratio of  $Fe^{3+}$  to  $Fe^{2+}$  ions, the pH, and the ionic strength [37].

For the synthesis of  $Fe_3O_4$ , a chemical co-precipitation process could be used, in which metal ions  $Fe^{3+}$  and  $Fe^{2+}$  were taken in a ratio of 2:0.5, and dodecylbenzenesulfonic acid was used as an emulsifier together with ammonia as a precipitant, which also ensured an alkaline medium [38].

In particular, in research paper [39], dispersed magnetite particles coated with sodium dodecyl sulfate were used for adsorption of the cationic basic dye blue 41. The maximum sorption capacity of this dye by this adsorbent (determined by the Langmuir model) was 2000.6 mg/g. Magnetite demonstrated itself positively as a sorbent applied to the surface of activated carbon [40]. The dyes sunset yellow, eosin B, and methylene blue were subjected to sorption. The short adsorption time of ~4–6 min to establish the adsorption equilibrium supported the use of ultrasound as an effective means to accelerate the adsorption of the corresponding dyes [18,40]. Thus, analyzing the already existing positive experience of using iron-containing sorbents, it is possible to assume and affirm the following: the use of dispersed iron-containing particles as a sorbent can reduce the size of the adsorber itself, in which the water treatment process takes place [13]. This is mainly due to the short time

required to reach adsorption equilibrium and the high values of the maximum sorption capacity [12].

So, it is important to continue these studies on creating the conditions that would allow one to obtain iron-containing magnetic materials of the required phase composition and particle sizes during the processing of industrial waste—exhausted etching solutions with minimal energy consumption. This is important for further use of these materials, in particular, for obtaining highly dispersed materials, such as sorbents.

The aim of this study was to analyze conditions for the formation of iron-containing compounds and their subsequent phase transformation under different conditions of the ferritization process for processing exhausted etching solutions. This will make it possible to determine the rational parameters for the application of energy-efficient ferritization for the formation of promising and safe magnetic compounds for further use, including magnetite and maghemite.

## 2. Materials and Methods

### 2.1. Experimental Set

The process of ferritization of exhausted etching solutions was studied in reactors with a working volume of 1 dm<sup>3</sup>, both with traditional thermal activation of the reaction mixture at a temperature of 75 °C and with energy-efficient alternating magnetic field (AMF) activation on the installation shown at Figure 1 at room temperature. To carry out AMF activation and to regulate its parameters, a controlled generator of rectangular pulses was developed based on the ATmega328p microcontroller board (Microchip Technology Inc., Chandler, AZ, USA). The output voltage of the pulses at 8 digital outputs of the controller board was 5 V, and the maximum current was 20 mA. Experimental parameters for pulse generation were set by the UTP3305C power supply unit via the RS-232 interface (Figure 1).



**Figure 1.** Laboratory ferritization installation with activation of the reaction mixture with alternating magnetic fields: 1—computer; 2—electronic block-case; 3—power supply; 4—electromagnetic coil with a steel core; 5—reactor with study solution.

This scheme allows one to form complex pulse packs consisting of a certain number of pulses and pauses between them of a specified duration. It is also possible to adjust the amplitude of individual pulses in the pack. Pack generation is provided by a program on a personal computer. In research paper [28], rational parameters for carrying out AMF activation were determined: the amplitude of the magnetic induction was 0.1 Tl, the pulse frequency was 1 Hz, the period between pulses was 100 ms, and the pulse duration was 1000 ms. These parameters were used in this study.

## 2.2. Study Materials

The input material for the production of iron-containing compounds by the ferritization method was an exhausted sulfuric acid etching solution for steel surfaces, which had a pH of 1.41 and a  $\text{FeSO}_4$  concentration of  $126.5 \text{ g/dm}^3$ . Both methods for the activation of the reaction mixture were used in the experiments. The variable factors of the ferritization process were the pH of the solution, the duration of the aeration process, and the initial concentrations of iron (II) ions in the reaction mixture (series of experiments A, B, and C, respectively, in Table 1). To achieve the necessary concentrations of iron (II) ions for ferritization, within the range of  $6.6$  to  $36.6 \text{ g/dm}^3$ , the exhausted etching solution was diluted with tap water. pH was adjusted with a 25% solution of sodium hydroxide to reach a certain pH value. Aeration of the reaction mixture was carried out with air oxygen at a rate of  $0.15 \text{ m}^3/\text{h}$ .

**Table 1.** Conditions for obtaining samples of ferritization precipitates.

Core Sample ID	pH of the Reaction Mixture	Concentration ( $\text{Fe}^{2+}$ ), $\text{g/dm}^3$	The Time of the Ferritization Process, min
A-1	8.5	16.6	15
A-2	9.5	16.6	15
A-3	10.5	16.6	15
A-4	11.5	16.6	15
B-1	11.5	16.6	5
B-2	11.5	16.6	10
B-3	11.5	16.6	15
B-4	11.5	16.6	20
B-5	11.5	16.6	25
B-6	11.5	16.6	30
C-1	11.5	46.6	15
C-2	11.5	36.6	15
C-3	11.5	26.6	15
C-4	11.5	16.6	15
C-5	11.5	6.6	15

After ferritization, a suspension was obtained, which was separated in a CM-5 centrifuge (Micromed, Poltava, Ukraine) with a separation factor of 3600 for 2 min. The sediment was dried for 24 h at a temperature of  $105 \text{ }^\circ\text{C}$  in an electric drying cabinet CHOЛ 67/350 (Ukraine) (Figure 2). A detailed description of the samples is presented in Table 1.

Phase analysis of dried powder samples of sediments was carried out by X-ray diffraction in step-by-step mode with Cu-K $\alpha$  radiation on a diffractometer Ultima IV (Rigaku, Japan). The scan was performed in the angular range of  $6$  to  $65^\circ 2\theta$  with a scanning step of  $0.05^\circ$  and an exposure time of 2 s per point. The diffractograms were interpreted using the ICDD PDF2+—2003 database (The International Centre for Diffraction Data) and the Match! V.1.9a software (Crystal Impact, Materials Park, OH, USA) [13,41].

The particle size of the precipitate samples was determined by the granulometric method using a laser analyzer Cilas 990 (Cilas, Orléans, France) in the measurement range from  $0.2$  to  $500 \text{ }\mu\text{m}$ . The error in determining the particle size on this device does not exceed 3%.



**Figure 2.** The sample of the obtained iron-containing sediment after ferritization of the etching solution.

The residual total concentration of iron ions in the solution after removal of the precipitate was determined using a DR3900 spectrophotometer (Hach, Loveland, CO, USA) with the use of Hach test kit No. 2608799. The pH value of the reaction mixture during ferritization was determined using a PL-700AL pH meter (Wrocław, Poland).

The evaluation of the dispersion and limits of errors of the experiments for determining the residual concentrations of iron ions after the ferritization process was carried out using the method [42] with a confidence probability of 0.95.

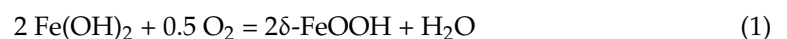
### 3. Results

#### 3.1. The Study of pH Influence

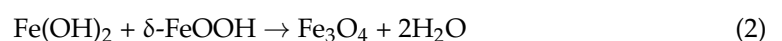
The study of the qualitative and quantitative composition of the ferritization precipitate was carried out with variable pH values of the reaction mixture and other constant parameters of the ferritization process. The concentration of iron ions in the reaction mixture was  $16.6 \text{ g/dm}^3$  and the duration of the ferritization process was 15 min.

In the process of ferritization, both with thermal and AMF activation of the reaction mixture, a dispersed black suspension was formed in the studied range of pH values, which later crystallized to form, mainly dense iron-containing structures in the precipitate. In the samples of precipitates, chemically stable ferromagnetic phases of magnetite  $\text{Fe}_3\text{O}_4$  and maghemite  $\gamma\text{-Fe}_2\text{O}_3$  with lattice parameters ( $a$ ) of 8.36 and 8.34 Å, respectively, were identified (Figure 3). It should be noted that, in addition to the formation of magnetite and maghemite, the precipitate also contains other solid-phase products of the ferritization reaction, including non-magnetic ferrihydrite  $\delta\text{-FeOOH}$ ,  $a = 2.95 \text{ Å}$ , which is less stable in alkaline media [43].

The structural studies of the samples (Figure 3) indicate the influence of the pH value and the method of activation of the reaction mixture on the phase composition of the precipitates. With an increase in the pH of the reaction mixture from 8.5 to 11.5, the following phase transformation is observed:  $\delta\text{-FeOOH} \rightarrow \text{Fe}_3\text{O}_4 \rightarrow \gamma\text{-Fe}_2\text{O}_3$  (Figure 3). It is noteworthy that the precipitates obtained at pH 8.5 contain a significant amount of ferrihydrite  $\delta\text{-FeOOH}$  (Table 2). The process of formation of this phase is a two-stage one: at the first stage of the process,  $\text{Fe}^{2+}$  ions form an unstable hydroxide  $\text{Fe}(\text{OH})_2$  in an oxidizing medium, which is then transformed into  $\delta\text{-FeOOH}$  by the following reaction:



In the reaction mixture with  $\text{pH} \geq 10$ , the precipitate contained predominantly the magnetite phase  $\text{Fe}_3\text{O}_4$ . Its formation at high pH values, in our opinion, is due to the rapid formation of iron hydroxide and oxyhydroxide with their subsequent transformation into the spinel structure of magnetite [44]. The mechanism of magnetite formation is obviously associated with the transformation of oxyhydroxides in the presence of  $\text{Fe}^{2+}$  hydroxide [45] according to the following reaction:



It should be noted that the divalent iron in magnetite is capable of further oxidation during aeration, transitioning to the more stable phase of maghemite according to the following reaction:



The structure of the resulting  $\gamma\text{-Fe}_2\text{O}_3$  is identical to the structure of  $\text{Fe}_3\text{O}_4$ ; both compounds have the inverse spinel structure, but maghemite is characterized by the presence of free vacancies distributed in the cation sublattice [24].

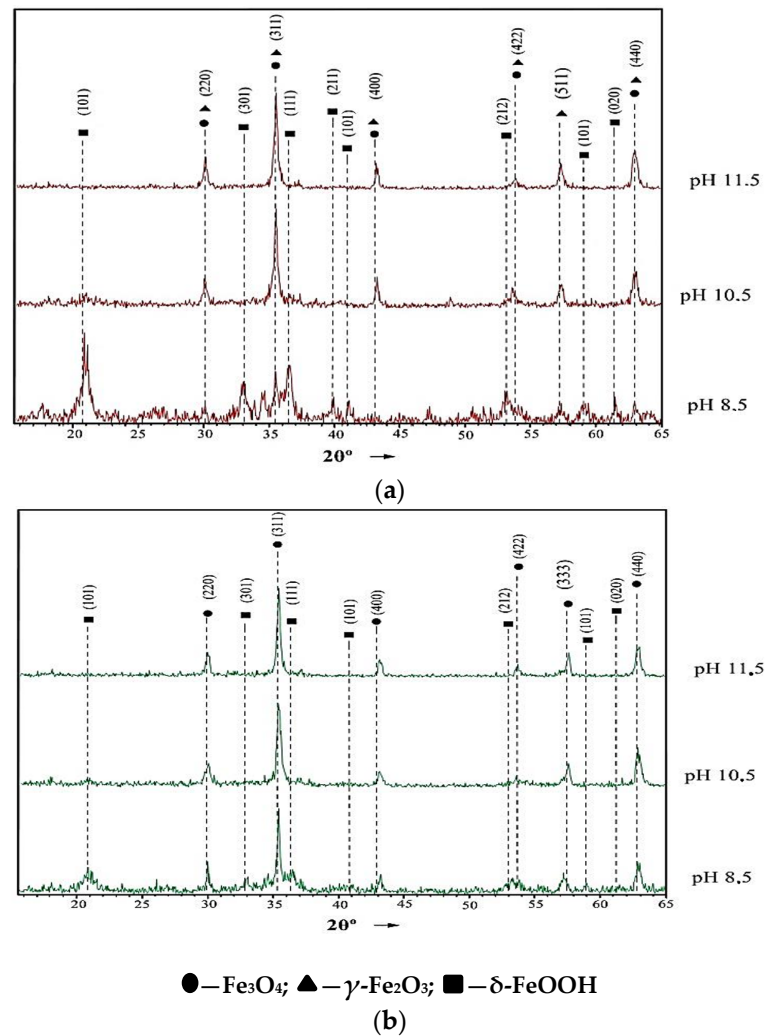


**Figure 3.** X-ray diffraction patterns of ferritization precipitates obtained at different pH values: (a) thermal activation; (b) AMF activation.

**Table 2.** Phase transformation in precipitates depends on pH and the method of activation of the reaction mixture.

Sample	pH	The Content of Inorganic Phase, % w/w				
		Thermal Activation			AMF Activation	
		$\delta\text{-FeOOH}$	$\text{Fe}_3\text{O}_4$	$\gamma\text{-Fe}_2\text{O}_3$	$\delta\text{-FeOOH}$	$\text{Fe}_3\text{O}_4$
A-1	8.5	75.4	24.6	–	61.1	38.9
A-2	9.5	35.3	64.7	–	37.8	62.2
A-3	10.5	2.7	97.3	–	9.1	90.9
A-4	11.5	–	81.1	18.9	–	100

It should be noted that at pH 11.5, with thermal activation of the ferritization reaction mixture, the final products in the precipitate are magnetite (81.1%) and maghemite (18.9%), and with AMF activation, a precipitate is obtained that contains only the magnetite phase. The results of the studies (Table 2) also show that AMF activation of the reaction mixture in the pH range of 8.5–11.5, compared to thermal activation, slows down the process of phase transformation in the precipitates. This may be due to the greater ability of thermal activation to initiate reactions of iron-containing compounds in the solution.

Phase studies are in good agreement with the data of chemical analysis of solutions obtained after the removal of ferritization precipitates. As the results of the studies showed, phase transformations of ferritic compounds in the precipitate and their stability in an alkaline medium have an impact on the content of residual concentrations of iron ions in the solution. Thus, after the ferritization of the reaction mixture with pH 8.5, the solution contains significant concentrations of iron ions ( $\text{Fe}^{2+}$  and  $\text{Fe}^{3+}$ ):  $34 \text{ mg/dm}^3$  with thermal and  $14 \text{ mg/dm}^3$  with AMF activation. With an increase in the pH values of the reaction mixture from 8.5 to 11.5, the total iron ion content of both activation methods decreases to  $0.78 \text{ mg/dm}^3$ . This is obviously explained by the fact that with an increase in the pH of the medium, the process of the transformation of unstable intermediate phases  $\text{Fe}(\text{OH})_2$  and  $\delta\text{-FeOOH}$  into more stable  $\text{Fe}_3\text{O}_4$  and  $\gamma\text{-Fe}_2\text{O}_3$  is accelerated.

### 3.2. Determination of the Effect of the Duration of Ferritization of the Reaction Mixture

The results of structural studies on the samples of precipitates obtained from a reaction mixture with a constant pH of 11.5 and different durations of aeration are presented in Figure 4 and Table 3. The obtained data indicate the influence of the time of the ferritization process on the phase composition of the precipitate. In the studied samples of precipitates (Figure 4), the following phases were identified:  $\gamma\text{-FeOOH}$ ,  $\delta\text{-FeOOH}$ ,  $\text{Fe}_3\text{O}_4$ , and  $\gamma\text{-Fe}_2\text{O}_3$ .

On the X-ray pattern of the sample of the precipitate obtained with a ferritization duration of 5 min with AMF activation, the reflexes  $2\theta = 20.7$  and  $33.6$  were recorded, which correspond to the diffraction maxima with indices (101) and (001) of the lepidocrocite phase  $\gamma\text{-FeOOH}$ .

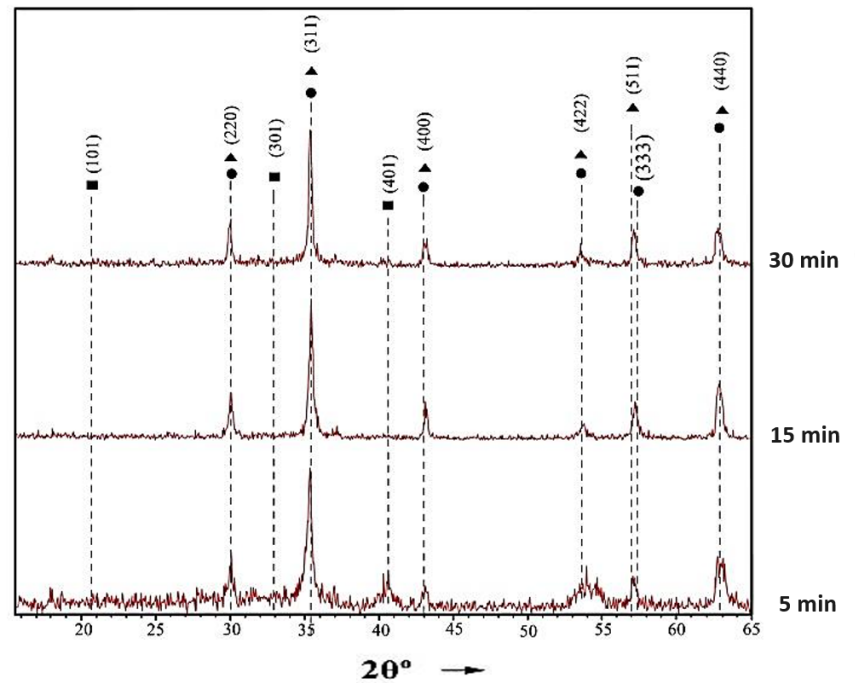
It should be noted that under the conditions of the ferritization process with a pH of 11.5, the reaction mixture ions of iron initially form  $\text{Fe}(\text{OH})_2$  with its subsequent transformation in an oxidizing medium into  $\text{Fe}(\text{OH})_3$ . The subsequent phase transformations of  $\text{Fe}(\text{OH})_3$  are associated with the processes of its structuring into iron oxyhydroxides according to the reaction:



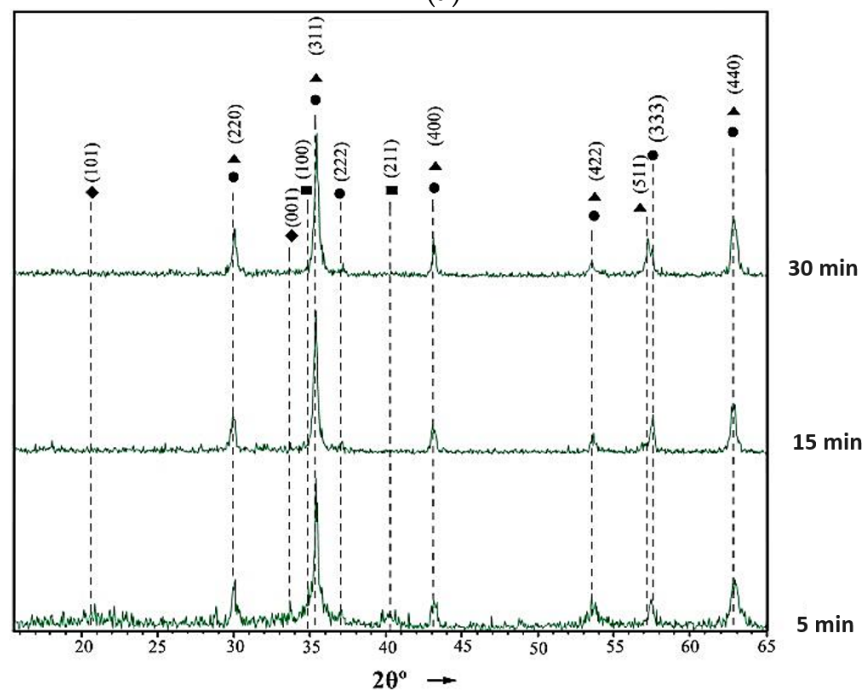
It should be noted that in the process of ferritization, iron hydroxides are transformed into oxyhydroxides of various structural modifications according to reactions (1) and (4). In addition, with thermal activation of the reaction mixture, the course of phase transformations with the formation of the phase of iron oxyhydroxides can occur at a ferritization duration of less than 5 min. On the X-ray diffraction pattern (Figure 3), at a ferritization duration of 15 min with thermal activation, a reflex is observed at an angle of  $2\theta = 57.5$ , which corresponds to the diffraction maximum with indices (333) of the  $\text{Fe}_3\text{O}_4$  phase. With the further course of the ferritization process for 30 min, this reflex is absent, which suggests the completion of the process of transforming  $\text{Fe}_3\text{O}_4$  into the  $\gamma\text{-Fe}_2\text{O}_3$  phase.

The analysis of the quantitative phase composition of precipitate samples (Table 3) showed that with an increase in the duration of the ferritization process with both methods of activation of the reaction mixture, there is a change in the contents of different iron-containing compounds. It should be noted that at a process duration of 5 min with both methods of activation, the mass fraction of the  $\text{Fe}_3\text{O}_4$  phase is more than 50%. The formation of only the magnetite phase from iron oxyhydroxides occurs during ferritization for 11 and 15 min using thermal and AMF activation, respectively. However, with further aeration of the reaction mixture, a complete or partial phase transformation of  $\text{Fe}_3\text{O}_4$  into  $\gamma\text{-Fe}_2\text{O}_3$  is reached.

Chemical analysis showed that the residual content of iron ions in the solution after 30 min of the ferritization process using both methods of activation of the reaction mixture does not exceed  $0.6 \text{ mg/dm}^3$ . The decrease in the residual concentrations of iron ions is obviously due to the formation of chemically stable phases of iron oxides in the precipitate, including magnetite and maghemite.



(a)



● –  $\text{Fe}_3\text{O}_4$ ; ▲ –  $\gamma\text{-Fe}_2\text{O}_3$ ; ■ –  $\delta\text{-FeOOH}$ ; ◆ –  $\gamma\text{-FeO(OH)}$

(b)

**Figure 4.** X-ray diffraction patterns of precipitates obtained at different durations of the ferritization process: (a) thermal activation; (b) AMF activation.

**Table 3.** Phase transformation depends on the duration of ferritization and the method of activation of the reaction mixture.

Sample	The Time of the Ferritization Process, min	The Content of Inorganic Phase, % w/w						
		Thermal Activation			AMF Activation			
		$\delta$ -FeOOH	Fe <sub>3</sub> O <sub>4</sub>	$\gamma$ -Fe <sub>2</sub> O <sub>3</sub>	$\gamma$ -FeOOH	$\delta$ -FeOOH	Fe <sub>3</sub> O <sub>4</sub>	$\gamma$ -Fe <sub>2</sub> O <sub>3</sub>
B-1	5	16.6	83.4	–	27.7	16.6	55.7	–
B-2	10	2.9	97.1	–	–	28.6	71.4	–
B-3	15	–	81.1	18.9	–	–	100	–
B-4	20	–	34.6	65.4	–	–	97.1	2.9
B-5	25	–	8.2	91.8	–	–	89.6	10.4
B-6	30	–	–	100	–	–	74.6	25.4

### 3.3. Determination of the Effect of the Initial Concentration of Iron Ions in the Reaction Mixture

The studies were carried out at constant ferritization parameters: a pH of the reaction mixture of 11.5 and a process duration of 15 min. The concentration of total iron varied in the range of 6.6 to 46.6 g/dm<sup>3</sup>.

Identification of phases in the obtained samples of precipitates suggested the presence of such compounds as  $\delta$ -FeOOH, Fe<sub>3</sub>O<sub>4</sub>, and  $\gamma$ -Fe<sub>2</sub>O<sub>3</sub> (Figure 5). It should be noted that at a significant concentration of iron ions in the reaction mixture—46.6 g/dm<sup>3</sup> and AMF activation, the precipitate contains a significant amount of intermediate solid-phase compounds, including non-magnetic ferrihydrite  $\delta$ -FeOOH. This sample is characterized by wide diffraction maxima of this phase, which is probably due to its low degree of crystallinity. Such structural features are explained by the fact that at high concentrations of iron in the reaction mixture ( $\geq 30$  g/dm<sup>3</sup>), the effect of electromagnetic discharges is insufficient for rapid initiation of the reaction in the concentrated reaction mixture with the formation of iron oxides with dense crystalline structure. Therefore, under the above-mentioned ferritization factors, the formation of intermediate, less chemically stable solid-phase compounds occurs to a significant extent. In addition, in the samples of the precipitate obtained at the initial iron concentration of 6.6 g/dm<sup>3</sup>, both methods of process activation identified narrow diffraction maxima of iron oxides of high intensity, which is obviously due to the high degree of crystallinity of their structure.

The results of the quantitative phase composition of the precipitate obtained at the initial concentration of Fe<sup>2+</sup> 46.6 g/dm<sup>3</sup> and AMF activation of the ferritization process confirm our assumptions about the presence of a significant content (>50%) of the chemically unstable phase of ferrihydrite  $\delta$ -FeOOH (Table 4). The end products of the phase formation process at the initial concentration of iron ions of 6.6 g/dm<sup>3</sup> and thermal activation consist exclusively of the maghemite phase and with AMF activation—magnetite (50.8%) and maghemite (49.2%).

**Table 4.** Phase transformation depends on the initial concentration of iron ions in the reaction mixture and the method of activation of the ferritization process.

Sample	Initial Concentration Fe(total), g/dm <sup>3</sup>	The Content of Inorganic Phase, % w/w					
		Thermal Activation			AMF Activation		
		$\delta$ -FeOOH	Fe <sub>3</sub> O <sub>4</sub>	$\gamma$ -Fe <sub>2</sub> O <sub>3</sub>	$\delta$ -FeOOH	Fe <sub>3</sub> O <sub>4</sub>	$\gamma$ -Fe <sub>2</sub> O <sub>3</sub>
C-1	46.6	29.2	70.8	–	55.8	44.2	–
C-2	36.6	14.1	85.9	–	35.5	64.5	–
C-3	26.6	–	100	–	10.9	89.1	–
C-4	16.6	–	81.1	18.9	–	100	–
C-5	6.6	–	–	100	–	50.8	49.2

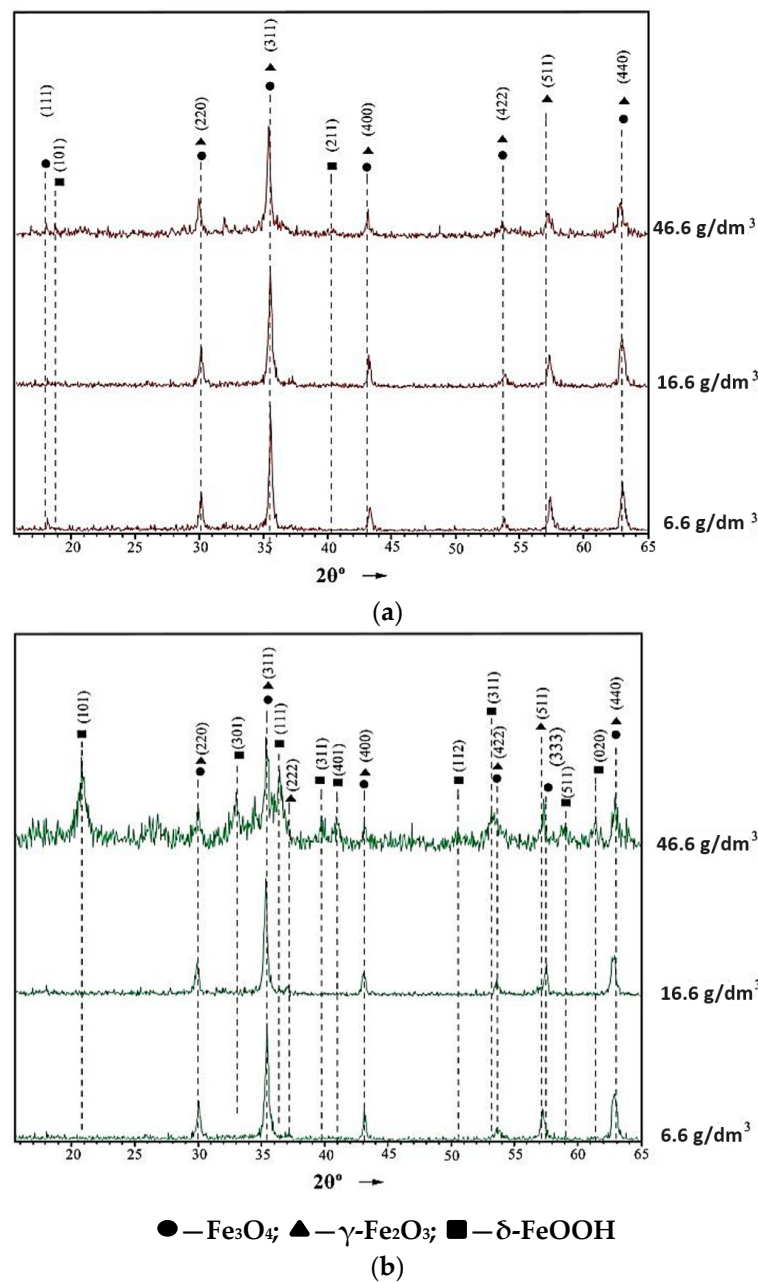


**Figure 5.** X-ray diffraction patterns of ferritization precipitates obtained at different initial concentrations of iron ions: (a) thermal activation; (b) AMF activation.

Chemical analysis of the solution after the precipitate was removed showed that the residual total iron content in the solution does not exceed  $0.3 \text{ mg/dm}^3$  at their initial concentration of  $6.6 \text{ g/dm}^3$  and use of both methods of activation of the reaction mixture. Such a high degree of wastewater treatment is obviously due to the fact that the purified solution is in contact with chemically stable solid phases of  $\text{Fe}_3\text{O}_4$  and  $\gamma\text{-Fe}_2\text{O}_3$ .

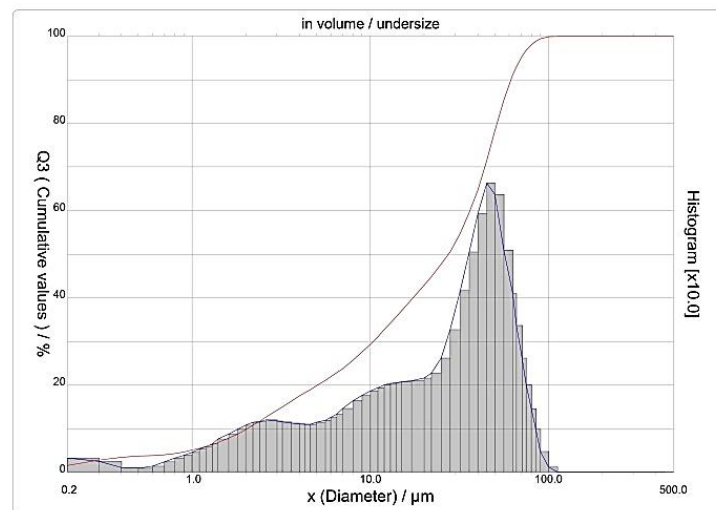
Note that the final solid-phase product of the ferritization process is a maghemite precipitate— $\gamma\text{-Fe}_2\text{O}_3$ . This one is a sufficiently stable compound that can only be irreversibly transformed into hematite  $\alpha\text{-Fe}_2\text{O}_3$  at high temperatures ( $300\div 500 \text{ }^\circ\text{C}$ ). Therefore, given the high chemical and thermal stability of hematite [46], it is the final stage of the transformation of iron oxides in an oxidizing environment.

### 3.4. Determination of the Average Particle Size of Precipitate Samples

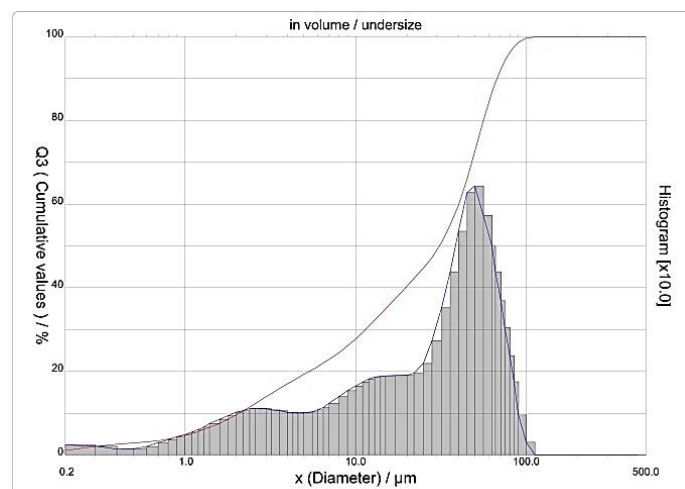
The particle sizes of the single-phase samples of magnetite precipitate  $\text{Fe}_3\text{O}_4$ , which were obtained by using both methods of activation of the reaction mixture, were also studied (Table 4). The results of the determination of the particle sizes of magnetite are shown in Table 5 and Figure 6. As can be seen from the data given in Table 5, their sizes are in the range of 1.90 to 61.55  $\mu\text{m}$ , and the average particle size is 29.62 and 27.79  $\mu\text{m}$  for thermal and AMF activation, respectively. The method of process activation and the initial concentration of iron ions in the reaction mixture do not significantly affect the particle sizes of magnetite. Thus, as a result of ferritization, a precipitate is formed, which consists of aggregates of particles of a ferrosphenel structure that are heterogeneous in size (Figure 6).

**Table 5.** Particle size of magnetite samples.

The Method of Activation	Particle Size, $\mu\text{m}$			
	Average Value	$D_{10,3}$	$D_{50,3}$	$D_{90,3}$
Thermal	29.62	2.03	27.36	61.55
AMF	27.69	1.90	23.62	59.05



(a)



(b)

**Figure 6.** Particle size distribution of magnetite samples obtained by different methods of activation of the ferritization process: (a) thermal; (b) AMF activation.

To prevent the formation of aggregates and increase the dispersity of the particles, ultrasonic treatment of the reaction mixture can be used after the completion of the aeration process. The high dispersity of magnetite particles and their uniformity are important factors for the further production of sorbents from these materials [47,48].

Dispersed magnetite particles with a size comparable to those obtained in this work can be synthesized by the method of electroerosive dispersion of steel chips [49]. With the additional use of ultrasound, the average particle size decreased to 9.1  $\mu\text{m}$ , indicating further dispersion of the magnetite samples during such a treatment. In view of this, our next studies will be aimed at studying the effect of ultrasound, as well as of surfactants, on the ferritization reaction mixture.

Thus, as predicted, the obtained results of experimental studies can be of particular importance in the field of wastewater treatment. The resulting nanoparticles with ferromagnetic properties can be particularly effective for water purification from various dyes. It is known that these types of pollution cause difficulties in their removal from water.

The obtained research results provide grounds for further perspective development of the study of the obtained sediments for the possibility of their use as adsorbents without and with chemical modification. Therefore, the first important stage of subsequent studies of the obtained samples will be the determination of the surface adsorption potential and the presence of various surface-active centers, which is expressed by the pH parameter, at which the cumulative charge of the adsorbent surface is zero, that is, it is called the point of zero charges (pHpzc) [18,50]. This will make it possible to better and more reasonably suggest the field of their application, i.e., for the treatment of which wastewaters they will be the most effective [51,52].

#### 4. Conclusions

Based on data from X-ray diffractometry, the processes of phase formation and regularities of transformations of oxyhydroxides  $\gamma\text{-FeOOH}$  and  $\delta\text{-FeOOH}$  and iron oxides  $\text{Fe}_3\text{O}_4$  and  $\gamma\text{-Fe}_2\text{O}_3$  were studied during the ferritization processing of spent pickling solutions. The effect of key technological factors, namely pH values and initial concentrations of  $\text{Fe}^{2+}$  in the reaction mixture as well as the duration of the ferritization process on the qualitative and quantitative composition of the precipitates were studied. Based on the results of quantitative analysis of the precipitates, the technological factors of the ferritization process were determined—the ones at which the formation of exclusively oxide phases of magnetite or maghemite is achieved.

The studies indicate that the application of energy-efficient activation of the reaction mixture by alternating magnetic fields slows down the process of formation and transformations of iron-containing phases. This activation method mainly leads to the formation of a magnetite precipitate— $\text{Fe}_3\text{O}_4$ . When using traditional thermal activation, the more stable maghemite phase  $\gamma\text{-Fe}_2\text{O}_3$  is mainly obtained. Data from laser granulometric analysis indicate the formation of ultradispersed heterogeneous magnetite particles in ferritization precipitates. The average size of these particles was determined to be 29.62 and 27.79  $\mu\text{m}$  for thermal and AMF activation, respectively. Such dispersed ferromagnetic materials can be promising for obtaining sorbents that are easily separated from the liquid phase on magnetic filters, but this requires careful further study.

It has been established that under conditions of the formation of stable solid phases of magnetite or maghemite, exhausted etching solutions treated by the ferritization method are suitable for reuse in industrial production processes since the total concentration of residual iron in them meets the current standards.

The results of the study showed that the ferritization process is a promising method for the treatment of exhausted etching solutions. Application of energy-efficient activation of the reaction mixture by alternating magnetic fields leads to the formation of ultradispersed magnetite precipitates, that can be used as sorbents.

**Author Contributions:** Conceptualization, D.S., G.K. and Y.T.; methodology, A.K., D.S. and G.K.; software, D.S., A.K. and D.C.; validation, G.K., Y.T. and D.C.; formal analysis, G.K. and Y.T.; investigation, Y.T.; resources, D.S., G.K., Y.T. and D.C.; data curation, D.S.; writing—original draft preparation, G.K. and D.C.; writing—review and editing, Y.T.; visualization, D.S., A.K. and D.C.; supervision, D.S.; project administration, D.S. and G.K.; funding acquisition, Y.T. All authors have read and agreed to the published version of the manuscript.

**Funding:** The authors would like to thank The Science and Technology Center in Ukraine for the support of research project NSEPEUR23002-1006 «Development of a new resource efficient technology for production of anti-corrosion coatings for civil infrastructure sites and analysis of possible options to spread the technology».

**Data Availability Statement:** The original contributions presented in the study are included in the article, further inquiries can be directed to the corresponding author.

**Conflicts of Interest:** The authors declare no conflict of interest.

## References

1. Brück, F.; Fritzsche, A.; Totsche, K.U.; Weigand, H. Steel Pickling Rinse Water Sludge: Concealed Formation of Cr(VI) Driven by the Enhanced Oxidation of Nitrite. *J. Environ. Chem. Eng.* **2017**, *5*, 2163–2170. [\[CrossRef\]](#)
2. Wieszczycka, K.; Filipowiak, K.; Wojciechowska, I.; Buchwald, T. Efficient Metals Removal from Waste Pickling Liquor Using Novel Task Specific Ionic Liquids—Classical Manner and Encapsulation in Polymer Shell. *Sep. Purif. Technol.* **2021**, *262*, 118239. [\[CrossRef\]](#)
3. Regel-Rosocka, M. A Review on Methods of Regeneration of Spent Pickling Solutions from Steel Processing. *J. Hazard. Mater.* **2010**, *177*, 57–69. [\[CrossRef\]](#)
4. Wiśniewski, J.; Wiśniewska, G. Acids and Iron Salts Removal from Rinsing Water after Metal Etching. *Desalination* **1997**, *109*, 187–193. [\[CrossRef\]](#)
5. Beni, A.A.; Esmaili, A. Biosorption, an Efficient Method for Removing Heavy Metals from Industrial Effluents: A Review. *Environ. Technol. Innov.* **2020**, *17*, 100503. [\[CrossRef\]](#)
6. Frank, J.J.; Poulakos, A.G.; Tornero-Velez, R.; Xue, J. Systematic Review and Meta-Analyses of Lead (Pb) Concentrations in Environmental Media (Soil, Dust, Water, Food, and Air) Reported in the United States from 1996 to 2016. *Sci. Total Environ.* **2019**, *694*, 133489. [\[CrossRef\]](#)
7. Sharma, R.; Shelke, S.; Bagheri Kashani, M.; Morose, G.; Christuk, C.; Nagarajan, R. Safer and Effective Alternatives to Perfluoroalkyl-Based Surfactants in Etching Solutions for the Semiconductor Industry. *J. Clean. Prod.* **2023**, *415*, 137879. [\[CrossRef\]](#)
8. Gueccia, R.; Winter, D.; Randazzo, S.; Cipollina, A.; Koschikowski, J.; Micale, G.D.M. An Integrated Approach for the HCl and Metals Recovery from Waste Pickling Solutions: Pilot Plant and Design Operations. *Chem. Eng. Res. Des.* **2021**, *168*, 383–396. [\[CrossRef\]](#)
9. Fadillah, G.; Yudha, S.P.; Sagadevan, S.; Fatimah, I.; Muraza, O. Magnetic Iron Oxide/Clay Nanocomposites for Adsorption and Catalytic Oxidation in Water Treatment Applications. *Open Chem.* **2020**, *18*, 1148–1166. [\[CrossRef\]](#)
10. Maliki, M.; Omorogbe, S.O.; Ifijen, I.H.; Aghedo, O.N.; Ighodaro, A. Incisive Review on Magnetic Iron Oxide Nanoparticles and Their Use in the Treatment of Bacterial Infections. In *TMS 2023 152nd Annual Meeting & Exhibition Supplemental Proceedings*; The Minerals, Metals & Materials Society, Ed.; The Minerals, Metals & Materials Series; Springer Nature: Cham, Switzerland, 2023; pp. 487–498. ISBN 978-3-031-22523-9.
11. Moreno, R.; Poyser, S.; Meilak, D.; Meo, A.; Jenkins, S.; Lazarov, V.K.; Vallejo-Fernandez, G.; Majetich, S.; Evans, R.F.L. The Role of Faceting and Elongation on the Magnetic Anisotropy of Magnetite Fe<sub>3</sub>O<sub>4</sub> Nanocrystals. *Sci. Rep.* **2020**, *10*, 2722. [\[CrossRef\]](#)
12. Trach, Y.; Tytkowska-Owerko, M.; Reczek, L.; Michel, M. Comparison the Adsorption Capacity of Ukrainian Tuff and Basalt with Zeolite–Manganese Removal from Water Solution. *J. Ecol. Eng.* **2021**, *22*, 161–168. [\[CrossRef\]](#)
13. Trach, Y.; Melnychuk, V.; Michel, M.M.; Reczek, L.; Siwiec, T.; Trach, R. The Characterization of Ukrainian Volcanic Tuffs from the Khmelnytsky Region with the Theoretical Analysis of Their Application in Construction and Environmental Technologies. *Materials* **2021**, *14*, 7723. [\[CrossRef\]](#)
14. Trach, Y.; Bujakowski, F.; Koda, E.; Mazur, L.; Nejbort, K.; Podlasek, A.; Vaverková, M.D. Characterization of Adsorbents from Ukrainian Kaolinite Clay for the Sorption of Nickel: Insight and Practical Application for Water Treatment in Conditions of Economic Constraints. *Desalination Water Treat.* **2022**, *278*, 1–12. [\[CrossRef\]](#)
15. Tanyildizi, M.Ş. Modeling of Adsorption Isotherms and Kinetics of Reactive Dye from Aqueous Solution by Peanut Hull. *Chem. Eng. J.* **2011**, *168*, 1234–1240. [\[CrossRef\]](#)
16. Šafaříková, M.; Šafařík, I. Magnetic Solid-Phase Extraction. *J. Magn. Magn. Mater.* **1999**, *194*, 108–112. [\[CrossRef\]](#)
17. Vozniuk, M.; Shabliy, T.; Gomelya, M.; Sirenko, L.; Sidorov, D. Magnetosorption Purification of Water from Petroleum Products. *J. Ecol. Eng.* **2023**, *24*, 155–162. [\[CrossRef\]](#) [\[PubMed\]](#)
18. Panda, S.K.; Aggarwal, I.; Kumar, H.; Prasad, L.; Kumar, A.; Sharma, A.; Vo, D.-V.N.; Van Thuan, D.; Mishra, V. Magnetite Nanoparticles as Sorbents for Dye Removal: A Review. *Environ. Chem. Lett.* **2021**, *19*, 2487–2525. [\[CrossRef\]](#)

19. Ma, Y.; Cheng, X.; Kang, M.; Yang, G.; Yin, M.; Wang, J.; Gang, S. Factors Influencing the Reduction of U (VI) by Magnetite. *Chemosphere* **2020**, *254*, 126855. [[CrossRef](#)] [[PubMed](#)]
20. Bai, S.; Zhu, S.; Jin, C.; Sun, Z.; Wang, L.; Wen, Q.; Ma, F. Sorption Mechanisms of Antibiotic Sulfamethazine (SMT) on Magnetite-Coated Biochar: PH-Dependence and Redox Transformation. *Chemosphere* **2021**, *268*, 128805. [[CrossRef](#)]
21. Drzymała, J. *Mineral Processing: Foundations of Theory and Practice of Minerallurgy*; University of Technology: Wrocław, Poland, 2007; ISBN 83-7493-362-3.
22. Natarajan, S.; Harini, K.; Gajula, G.P.; Sarmento, B.; Neves-Petersen, M.T.; Thiagarajan, V. Multifunctional Magnetic Iron Oxide Nanoparticles: Diverse Synthetic Approaches, Surface Modifications, Cytotoxicity towards Biomedical and Industrial Applications. *BMC Mater.* **2019**, *1*, 2. [[CrossRef](#)]
23. Kouotou, P.M.; Tian, Z.-Y. Controlled Synthesis of  $\alpha$ -Fe<sub>2</sub>O<sub>3</sub>@Fe<sub>3</sub>O<sub>4</sub> Composite Catalysts for Exhaust Gas Purification. *Proc. Combust. Inst.* **2019**, *37*, 5445–5453. [[CrossRef](#)]
24. Ali, A.; Zafar, H.; Zia, M.; Ul Haq, I.; Phull, A.R.; Ali, J.S.; Hussain, A. Synthesis, Characterization, Applications, and Challenges of Iron Oxide Nanoparticles. *Nanotechnol. Sci. Appl.* **2016**, *9*, 49–67. [[CrossRef](#)] [[PubMed](#)]
25. Gingasu, D.; Culita, D.C.; Calderon Moreno, J.M.; Marinescu, G.; Bartha, C.; Oprea, O.; Preda, S.; Chifiriuc, M.C.; Popa, M. Synthesis of CoFe<sub>2</sub>O<sub>4</sub> through Wet Ferritization Method Using an Aqueous Extract of Eucalyptus Leaves. *Coatings* **2023**, *13*, 1250. [[CrossRef](#)]
26. Frolova, L.A. The Mechanism of Nickel Ferrite Formation by Glow Discharge Effect. *Appl. Nanosci.* **2019**, *9*, 845–852. [[CrossRef](#)]
27. Kochetov, G.; Samchenko, D.; Lastivka, O.; Derecha, D. Determining the Rational Parameters for Processing Spent Etching Solutions by Ferritization Using Alternating Magnetic Fields. *East. Eur. J. Enterp. Technol.* **2022**, *3*, 21–28. [[CrossRef](#)]
28. Samchenko, D.; Kochetov, G.; Derecha, D.O.; Skirta, Y.B. Sustainable Approach for Galvanic Waste Processing by Energy-Saving Ferritization with AC-Magnetic Field Activation. *Cogent Eng.* **2022**, *9*, 2143072. [[CrossRef](#)]
29. Frolova, L.; Pivovarov, A.; Anisimova, L.; Yakubovskaya, Z.; Yakubovskii, A. The Extraction of Chromium (III) from Concentrated Solutions by Ferrite Method. *Voprosy Khimii Khimicheskoi Tekhnologii* **2017**, *6*, 110–115.
30. Kochetov, G.; Samchenko, D.; Arhatenko, T. Determination of Influence of PH on Reaction Mixture of Ferritization Process with Electromagnetic Pulse Activation on the Processing of Galvanic Sludge. *East. Eur. J. Enterp. Technol.* **2021**, *4*, 24–30. [[CrossRef](#)]
31. Heuss-Aßbichler, S.; John, M.; Klapper, D.; Bläß, U.W.; Kochetov, G. Recovery of Copper as Zero-Valent Phase and/or Copper Oxide Nanoparticles from Wastewater by Ferritization. *J. Environ. Manag.* **2016**, *181*, 1–7. [[CrossRef](#)]
32. Ying, Y.; Xiong, X.; Wang, N.; Zheng, J.; Yu, J.; Li, W.; Qiao, L.; Cai, W.; Li, J.; Huang, H.; et al. Low Temperature Sintered MnZn Ferrites for Power Applications at the Frequency of 1 MHz. *J. Eur. Ceram. Soc.* **2021**, *41*, 5924–5930. [[CrossRef](#)]
33. John, M.; Heuss-Aßbichler, S.; Tandon, K.; Ullrich, A. Recovery of Ag and Au from Synthetic and Industrial Wastewater by 2-Step Ferritization and Lt-Delafossite Process via Precipitation. *J. Water Process Eng.* **2019**, *30*, 100532. [[CrossRef](#)]
34. Yemchura, B.; Kochetov, G.; Samchenko, D.; Prikhna, T. Ferritization-Based Treatment of Zinc-Containing Wastewater Flows: Influence of Aeration Rates. In *Recent Advances in Environmental Science from the Euro-Mediterranean and Surrounding Regions*, 2nd ed.; Ksibi, M., Ghorbal, A., Chakraborty, S., Chaminé, H.I., Barbieri, M., Guerriero, G., Hentati, O., Negm, A., Lehmann, A., Römbke, J., et al., Eds.; Environmental Science and Engineering; Springer International Publishing: Cham, Switzerland, 2021; pp. 171–176. ISBN 978-3-030-51209-5.
35. Shariati, S.; Faraji, M.; Yamini, Y.; Rajabi, A.A. Fe<sub>3</sub>O<sub>4</sub> Magnetic Nanoparticles Modified with Sodium Dodecyl Sulfate for Removal of Safranin O Dye from Aqueous Solutions. *Desalination* **2011**, *270*, 160–165. [[CrossRef](#)]
36. Hasany, S.F.; Ahmed, I.; Rajan, J.; Rehman, A. Systematic Review of the Preparation Techniques of Iron Oxide Magnetic Nanoparticles. *Nanosci. Nanotechnol.* **2013**, *2*, 148–158. [[CrossRef](#)]
37. Laurent, S.; Forge, D.; Port, M.; Roch, A.; Robic, C.; Vander Elst, L.; Muller, R.N. Magnetic Iron Oxide Nanoparticles: Synthesis, Stabilization, Vectorization, Physicochemical Characterizations, and Biological Applications. *Chem. Rev.* **2008**, *108*, 2064–2110. [[CrossRef](#)] [[PubMed](#)]
38. Muhammad, A.; Shah, A.-H.A.; Bilal, S.; Rahman, G. Basic Blue Dye Adsorption from Water Using Polyaniline/Magnetite (Fe<sub>3</sub>O<sub>4</sub>) Composites: Kinetic and Thermodynamic Aspects. *Materials* **2019**, *12*, 1764. [[CrossRef](#)] [[PubMed](#)]
39. Yamini, Y.; Faraji, M.; Rajabi, A.A.; Nourmohammadian, F. Ultra Efficient Removal of Basic Blue 41 from Textile Industry's Wastewaters by Sodium Dodecyl Sulphate Coated Magnetite Nanoparticles: Removal, Kinetic and Isotherm Study. *Anal. Bioanal. Chem. Res.* **2018**, *5*, 205–215. [[CrossRef](#)]
40. Bagheri, A.R.; Ghaedi, M.; Asfaram, A.; Bazrafshan, A.A.; Jannesar, R. Comparative Study on Ultrasonic Assisted Adsorption of Dyes from Single System onto Fe<sub>3</sub>O<sub>4</sub> Magnetite Nanoparticles Loaded on Activated Carbon: Experimental Design Methodology. *Ultrason. Sonochem.* **2017**, *34*, 294–304. [[CrossRef](#)] [[PubMed](#)]
41. Trach, Y.; Melnychuk, V.; Stadnyk, O.; Trach, R.; Bujakowski, F.; Kiersnowska, A.; Rutkowska, G.; Skakun, L.; Szer, J.; Koda, E. The Possibility of Implementation of West Ukrainian Paleogene Glauconite–Quartz Sands in the Building Industry: A Case Study. *Sustainability* **2023**, *15*, 1489. [[CrossRef](#)]
42. McIllece, J.J. *On Generalized Variance Functions for Sample Means and Medians*; U.S. Bureau of Labor Statistics: Washington, DC, USA, 2018.
43. Pereira, D.I.A.; Bruggraber, S.F.A.; Faria, N.; Poots, L.K.; Tagmount, M.A.; Aslam, M.F.; Frazer, D.M.; Vulpe, C.D.; Anderson, G.J.; Powell, J.J. Nanoparticulate Iron(III) Oxo-Hydroxide Delivers Safe Iron That Is Well Absorbed and Utilised in Humans. *Nanomed. Nanotechnol. Biol. Med.* **2014**, *10*, 1877–1886. [[CrossRef](#)]

44. Dong, W.; Ding, J.; Wang, W.; Zong, L.; Xu, J.; Wang, A. Magnetic Nano-Hybrids Adsorbents Formulated from Acidic Leachates of Clay Minerals. *J. Clean. Prod.* **2020**, *256*, 120383. [[CrossRef](#)]
45. Lei, W.; Liu, Y.; Si, X.; Xu, J.; Du, W.; Yang, J.; Zhou, T.; Lin, J. Synthesis and Magnetic Properties of Octahedral Fe<sub>3</sub>O<sub>4</sub> via a One-Pot Hydrothermal Route. *Phys. Lett. A* **2017**, *381*, 314–318. [[CrossRef](#)]
46. Anigrahawati, P.; Sahar, M.R.; Sazali, E.S. Physical, Structural and Spectroscopic Analysis of Tellurite Glass Containing Natural Magnetite Fe<sub>3</sub>O<sub>4</sub> Nanoparticles. *Mater. Chem. Phys.* **2022**, *286*, 126183. [[CrossRef](#)]
47. Lv, W.; Liu, B.; Luo, Z.; Ren, X.; Zhang, P. XRD Studies on the Nanosized Copper Ferrite Powders Synthesized by Sonochemical Method. *J. Alloys Compd.* **2008**, *465*, 261–264. [[CrossRef](#)]
48. Choudhary, A.; Khandelwal, N.; Ganie, Z.A.; Darbha, G.K. Influence of Magnetite and Its Weathering Originated Maghemite and Hematite Minerals on Sedimentation and Transport of Nanoplastics in the Aqueous and Subsurface Environments. *Sci. Total Environ.* **2024**, *912*, 169132. [[CrossRef](#)] [[PubMed](#)]
49. Prikhna, T.; Monastyrov, M.; Soldatov, I.; Büchner, B.; Giebeler, L.; Sathyadharma Prasad, A.; Ostash, O.; Moshchil, V.; Podhurska, V.; Potapov, P.; et al. Corrosion-Resistant Polymer-Based Nanocomposite Materials with a High Level of Microwave Absorption and Soft Magnetic Materials Based on Iron Oxide Nanopowder Obtained by Electroerosion Dispersion. *Ceram. Int.* **2023**, *49*, 24322–24331. [[CrossRef](#)]
50. Kallay, N.; Preočanin, T. Measurement of the Surface Potential of Individual Crystal Planes of Hematite. *J. Colloid Interface Sci.* **2008**, *318*, 290–295. [[CrossRef](#)] [[PubMed](#)]
51. Dimirkou, A.; Ioannou, A.; Doula, M. Preparation, Characterization and Sorption Properties for Phosphates of Hematite, Bentonite and Bentonite–Hematite Systems. *Adv. Colloid Interface Sci.* **2002**, *97*, 37–61. [[CrossRef](#)]
52. Cromières, L.; Moulin, V.; Fourest, B.; Giffaut, E. Physico-Chemical Characterization of the Colloidal Hematite/Water Interface: Experimentation and Modelling. *Colloids Surf. Physicochem. Eng. Asp.* **2002**, *202*, 101–115. [[CrossRef](#)]

**Disclaimer/Publisher’s Note:** The statements, opinions and data contained in all publications are solely those of the individual author(s) and contributor(s) and not of MDPI and/or the editor(s). MDPI and/or the editor(s) disclaim responsibility for any injury to people or property resulting from any ideas, methods, instructions or products referred to in the content.